Multi-tip nano-prisms: Controlled growth and emission enhancement properties

2013 EPL 104 18004

(http://iopscience.iop.org/0295-5075/104/1/18004)

A Letters Journal Exploring the Frontiers of Physics

October 2013

EPL, **104** (2013) 18004
doi: 10.1209/0295-5075/104/18004

www.epljournal.org

Multi-tip nano-prisms: Controlled growth and emission enhancement properties

Ming Liu[1], Cong Meng[1], Zheng-Hong Xue[1], Xiang Xiong[1], Da-Jun Shu[1], Ru-Wen Peng[1], Qiang Wu[2], Zheng Hu[2] and Mu Wang[1(a)]

[1] *National Laboratory of Solid State Microstructures and Department of Physics, Nanjing University Nanjing 210093, China*
[2] *Key Laboratory of Mesoscopic Chemistry of MOE, School of Chemistry and Chemical Engineering, Nanjing University - Nanjing 210093, China*

received 28 June 2013; accepted in final form 30 September 2013
published online 28 October 2013

PACS 81.10.Bk – Growth from vapor
PACS 79.70.+q – Field emission, ionization, evaporation, and desorption
PACS 85.35.-p – Nanoelectronic devices

Abstract – We report here the experimental observations that the tip topography of ZnO nano-prisms sensitively depends on the percentage of oxygen in the flux of the carrying gas in vapor growth. At a relatively high oxygen concentration, a number of thin filaments can be nucleated atop nano-prisms, forming a unique fish-spear–like multi-tip morphology. The length and density of the "spear tines" depend on the flux of the carrying gas. The field emission properties of the nanorod array with different tip morphology are investigated. The structures with longer and denser spear tines possess lower turn-on electric field and higher electric current density. The cathodoluminescence properties of the ZnO nano-prisms have also been studied. The luminescence related to defects in multi-tip nano-prisms possesses the strongest intensity, and the nanorod without any tine structure possesses the lowest defect luminescence intensity. The intrinsic luminescence of ZnO around 385 nm, however, has the opposite tendency. We suggest that our observation is inspiring in optimizing the emission properties of the nanowire devices.

One-dimensional (1D) nanostructures have attracted much attention due to their unique applications in mesoscopic physics and nanodevices [1–5]. Field emission is one of the most fascinating properties of nano-prisms (and nanowires) and has been extensively studied [5–10]. One of the essential requirements for the field emission application is the large aspect ratio of the length *vs.* the cross-section area of the nanorod [11–13]. ZnO is an interesting material with very rich microscopic morphologies depending on the growth conditions [14]. For example, we once found that the cross-section size of a ZnO nanorod can be precisely tuned by controlling the growth temperature [15]. In addition to the advantages of the large aspect ratio and easy fabrication, ZnO possesses a wide bandgap energy of 3.37 eV and a large exciton binding energy of 60 meV [16]. It has excellent piezoelectric and emission properties with high thermal stability [17,18]. These features make ZnO nano-prisms promising for applications in field emission devices, photocatalysts and sensors.

The physical properties of ZnO nanostructures also depend on their topological features. It has recently been found that the ZnO hierarchical nanostructures characterized by a hexagonal central trunk with thin blades can be induced by repeated polytypism of wurtzite (WZ) and zinc-blende (ZB) phases [19]. The periodic blades provide the essential boundary conditions to establish resonant electromagnetic responses and lead to directional transmission of light [19]. To improve the field emission properties of ZnO nano-prisms, it would be helpful to generate even higher aspect ratio of the nano-prisms and realize higher field emission efficiency [20].

In this letter we report that the tip topography of ZnO nano-prisms sensitively depends on the percentage of oxygen in the flux of the nitrogen carrying gas in vapor growth. At a relatively high concentration of oxygen, a number of thin ZnO filaments can be nucleated atop the nano-prisms, forming a unique fish-spear–like morphology. The field emission properties of the nano-prism array depend on the density and the length of the tines: the

(a) E-mail: muwang@nju.edu.cn (corresponding author)

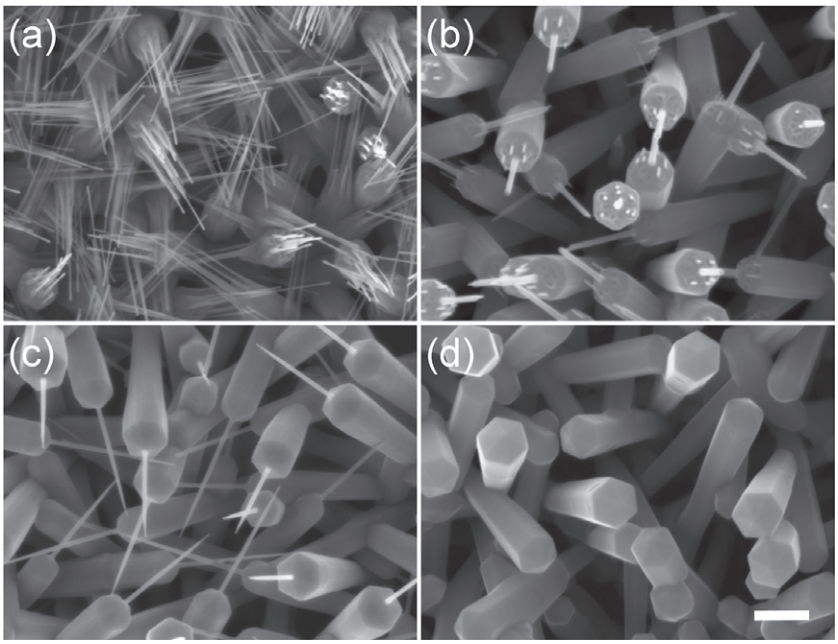

Fig. 1: FESEM micrographs of the tips of ZnO nano-prisms with different growth condition. After growing ZnO nano-prisms for 60 minutes, the oxygen supply is stopped. The residue oxygen in the furnace supports the growth of ZnO for a while. The growth morphology then depends on the nitrogen carrying gas. (a) The morphology of the ZnO nano-prisms grown when the flux of the nitrogen carrying gas resumes 300 sccm. (b) The morphology of the nano-prisms when the flux of the nitrogen carrying gas is increased to 400 sccm. (c) The morphology of nano-prisms when the flux of the nitrogen carrying gas is increased to 500 sccm. (d) The morphology of nano-prisms when the flux of the nitrogen carrying gas is further increased to 1800 sccm. The duration of the growth for the structures shown in (a)–(d) is 20 min. The bar represents 300 nm.

structures with longer and denser tines possess lower turn-on field strength and higher field emission current density. It is also observed that the cathodoluminescence properties of the ZnO nano-prisms with different tip morphologies are different. The luminescent peak related to the defects in multi-tined nano-prisms possesses the strongest intensity, whereas for the nano-prism without any tines, this peak is very weak. The intrinsic luminescence of ZnO at 385 nm, however, has the opposite tendency: the luminescence from the nano-prisms without any tine structure atop possesses the strongest intensity, whereas the luminescence from multi-tined tips is the weakest at 385 nm.

Zinc oxide single-crystalline nano-prisms are grown on Si(100) substrate by chemical vapor deposition with zinc powder (99.9%, Alfa Aesar) in nitrogen atmosphere with a trace amount of oxygen gas. No catalyst has been introduced in our experiments. A horizontal tube furnace is applied to grow ZnO nano-prisms, with ultrapure nitrogen gas as the carrying gas. The zinc powder is placed in a quartz boat, and the cleaned silicon substrates are placed upstream of the zinc powder. Before the experiment a large flux of N_2 flows through the furnace for one hour to remove the residue air therein. Then the furnace is heated to 600 °C (measured at the site close to the sample) at a rate of 20 °C/min and is kept at 600 °C with the N_2 flux as 300 sccm. A trace amount of ultrapure oxygen gas is then introduced (3 sccm). This process is kept for 60 minutes. The flux of O_2 is then cut off, yet the nitrogen flow is kept with a certain flux (the N_2 flux is selected as 300, 400, 500, 1800 sccm, respectively) at 600 °C for 20 min. The tip morphology sensitively depends on the nitrogen flux in the stage when the O_2 flux has been cut off (this means that the average concentration of the residue oxygen is modified in the furnace). The grown ZnO nano-prisms are characterized with a field emission scanning electron microscope (FESEM, LEO 1530VP). X-ray diffraction (XRD) analysis is carried out with a Bruker AXS D8 with monochromatic Cu $K\alpha$ radiation. The cathodoluminescence (CL) of the nano-prisms is measured at room temperature with the MonoCL3+ system (GATAN Instrument) installed in a field emission scanning electron microscope (ZEISS Ultra 55), and the electric field emission property of ZnO nano-prisms is characterized by a homemade setup with parallel-plate electrodes in a vacuum chamber (1.8×10^{-4} Pa) [21]. The separation of the parallel plates is kept as 150 μm, and the voltage applied across the plates is up to 3500 volts.

The ZnO nano-prisms grown with a different nitrogen flux at the later stage of growth are shown in fig. 1. Meanwhile, the O_2 supply has been cut off. If the nitrogen flux is kept as 300 sccm, we observe that some straight thin ZnO filaments are generated atop the previously grown prism, with their axis parallel to that of the original one, and forming a fish-spear–like pattern (fig. 1(a)). Each tine of the fish spear looks uniform, with a stem size smaller

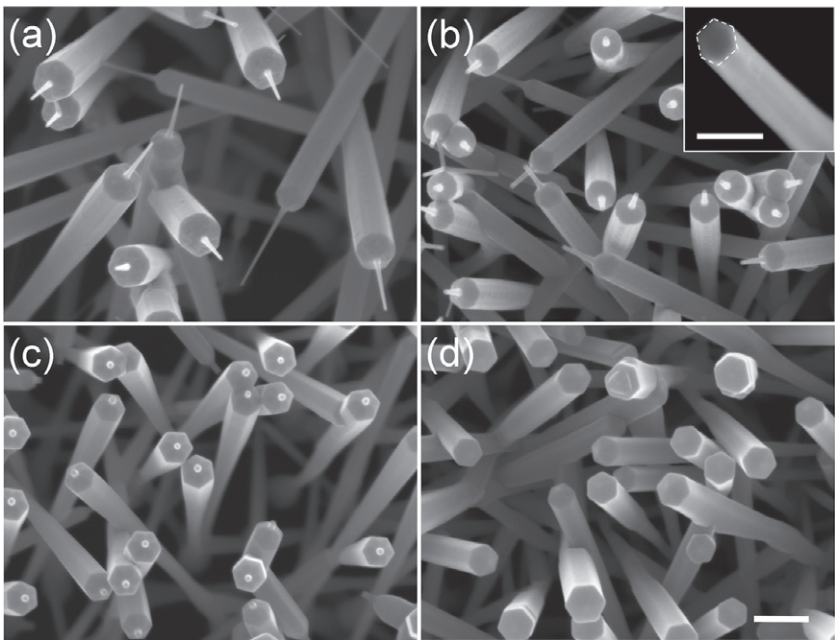

Fig. 2: FESEM micrographs of ZnO nano-prisms with different length of the filament atop. After cutting off the O_2 supply, the flux of the N_2 carrying gas is increased to 500 sccm, and the sample is kept growing with the residue oxygen for (a) 460 s, (b) 180 s, (c) 30 s, (d) 0 s, respectively. Then a large flux of N_2 gas (about 5000 sccm) is blown into the furnace to terminate the growth instantly. The scale bar in (d) represents 450 nm, and is valid for each frame (a)–(d). The bar in the inset of (b) represents 80 nm.

than 30 nm and the very central tine longer than the surrounding ones, as shown in fig. 1(a). The average length of the tines can reach several hundreds of nanometers. By increasing the flux of nitrogen to 400 sccm, as illustrated in fig. 1(b), the central tine of the "fish spear" keeps growing, and the surrounding tines become nucleated, yet they are not able to develop into long filaments. Further increasing the flux of the nitrogen carrying gas to 500 sccm after cutting off the oxygen supply, we observe that only the very central tine has been nucleated and develops atop the ZnO prism, no new filaments are generated in the surrounding area, as shown in fig. 1(c). If the flux of the N_2 carrying gas is further increased to 1800 sccm, nothing can be nucleated atop the nano-prisms, as illustrated in fig. 1(d).

It is interesting to investigate the evolution of tip topography as a function of time. To get the growth morphology at a specific moment, we intentionally blow in 5000 sccm N_2 to cease the growth instantly at a specific moment. The procedure of the experiment is designed as follows. After the initial growth of ZnO nano-prisms for 60 min, the flux of O_2 is cut off while the flux of N_2 is set as 500 sccm. After a certain period, a large amount of N_2 (5000 sccm) is blown through the furnace to terminate the growth. Figures 2(a)–(c) show the observed morphology when the growth is terminated in 460 s, 180 s, 30 s, respectively, where the average length of the thin filament is measured as 470 nm, 220 nm, and 12 nm, accordingly. The cross-section of the tine is hexagonal, as illustrated by the enlarged FESEM micrograph in the inset of fig. 2(b). Figure 2(d) shows the control experiment in which a large flux of N_2 gas is blown through the furnace immediately after the termination of the oxygen flux. One may find that nothing develops atop the prisms in this case. The relationship of the length of the tine as a function of time has been systematically investigated (fig. 3). One may find that the filament length is about to saturate at a certain value (in our experiment, this value is around 500 nm). This effect could be related to the fact that the oxygen supply in the system is limited (when the O_2 flux is cut off, the residue oxygen in the furnace is continuously decreasing), therefore the growth of filament atop the nano-prism cannot be sustained for a very long period.

The structure of the as-grown ZnO nano-prisms has been investigated by XRD. A typical XRD pattern of these samples is shown in fig. 4. The diffraction peaks can be indexed to hexagonal wurtzite ZnO ($a = 0.3249$ nm, $c = 0.5206$ nm). The observation of a strong (002) ZnO diffraction peak indicates that the nano-prisms are preferentially orientated along the c-axis. Previous crystallography studies have shown that the side facets of the hexagonal prism of ZnO are usually $(10\bar{1}0)$ or $(11\bar{2}0)$, which possess low surface energy [3]. The facets atop the prism have higher surface energy (for the scenario in which the side facets are $(11\bar{2}0)$, the facets atop the prism are $(11\bar{2}n)$, with n equal to 1, or 2, or 3 usually). According to the traditional theory of nucleation [22], it is easier to induce nucleation on a surface with higher energy. This explains that the fish-spear–like tine appears only on the facets atop the prism of ZnO.

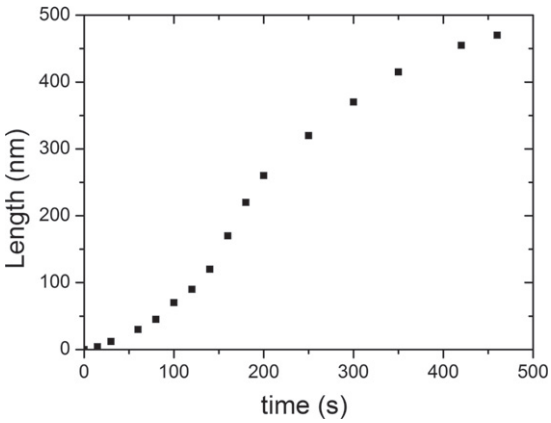

Fig. 3: The average length of the single filament atop the nano-prism *vs.* the growth time. The length of the filament increases first, yet it is about to saturate when the growth time exceeds 400 s.

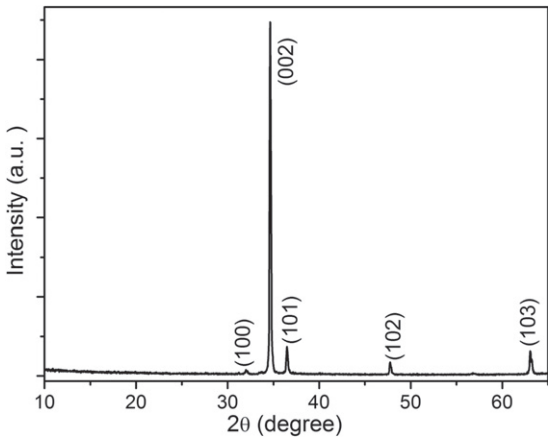

Fig. 4: XRD pattern obtained from the ZnO nano-prisms as that shown in fig. 1(d).

As illustrated in figs. 1(b) and (c), among the tines on the tip of ZnO prism, the one in the very center atop the prism is usually longer than the surrounding ones, suggesting that it must have been nucleated at a much earlier stage. This effect may be related to the fact that at the center atop the prism, there may exist a small (0001) facet [23,24], which is a Zn-terminated surface. Due to the self-catalyst effect of Zn atoms, nucleation on the Zn-terminated surface occurs preferentially [19].

The mechanism according to which the fish-spear–like tines are generated when the oxygen supply has been stopped, as that shown in figs. 1–3, can be understood as follows. We expect that the surface diffusion of oxygen or ZnO molecules absorbed on the facets atop the prism is slowed down when the oxygen supply is stopped [25]. According to the classic nucleation theory, the nucleus density increases with increasing ratio of the deposition rate to the surface diffusion rate [26]. Therefore, when the oxygen supply is stopped, the higher nucleus density contributes to the generation of a number of tines on the

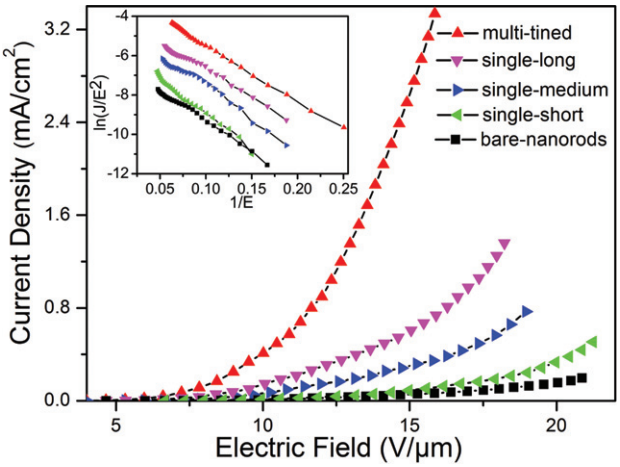

Fig. 5: (Colour on-line) Field emission current density measured as a function of the applied electric field for ZnO nano-prisms with different tip morphologies. The inset shows the plot of $\ln(J/E^2)$ *vs.* E^{-1}. The linear relationship between $\ln(J/E^2)$ and E^{-1} can be identified. It can be seen that the multi-tined nano-prisms have the highest emission efficiency.

facets atop the prism. The stronger flux of nitrogen, however, will blow away the oxygen in the furnace and decrease the oxygen adatoms or ZnO molecules adsorbed on the facets, and will decrease the deposition rate. This eventually leads to the phenomenon shown in fig. 1.

The field emission electric current from ZnO nano-prisms with different tip morphology has been measured with a two-parallel-plate scheme in a vacuum chamber with pressure 1.8×10^{-4} Pa at room temperature. The sample (ZnO nano-prisms on silicon substrate) is connected to the cathode, and the anode is a parallel stainless-steel plate. A voltage of 3 kV is applied before each measurement to degas the sample surface. The field emission electric current is measured by applying a voltage across the electrodes from 300 V to 3500 V with a sweep step of 100 V. The measured field emission current density *vs.* the applied electric field (J-E) is plotted in fig. 5 for samples with different tip morphologies.

At a fixed applied electric field, one may find that the emission current density is the highest for the fish-spear–like multi-tined tips; for the tip with a single tine, the emission current density depends on the length of the tine: the longer the tine atop, the higher the emission current density. The nano-prisms without any tines atop are most inefficient in generating the emission electric current. Quantitatively, the analysis of fig. 5 shows that the turn-on field ($E_{\rm on}$), which is defined as the required applied field to generate an emission current above $10\,\mu{\rm A/cm^2}$, is about $5.36\,{\rm V}/\mu{\rm m}$, $6.37\,{\rm V}/\mu{\rm m}$, and $10.2\,{\rm V}/\mu{\rm m}$, for the fish-spear–like tip with multiple tines (as that shown in fig. 1(a)), the tip with a long individual tine (as that shown in fig. 2(a)) and the nanorod without any filaments atop (as that shown in fig. 2(d)), respectively. The threshold field ($E_{\rm th}$), which is defined as the applied electric field

when the emission electric current reaches 1.0 mA/cm^2, is measured as 12.3 V/μm and 17.2 V/μm for the fish-spear–like tip with multiple tines (fig. 1(a)) and the tip with a long individual tine (fig. 2(a)), respectively. The threshold field for nano-prisms without any tine atop is so high that it is far beyond the applicable voltage range of our present facility.

According to the Fowler-Nordheim theory [27], field emission is essentially a result of tunneling of electrons through the potential barrier at the interface between the semiconductor and the vacuum. The strong applied electric field lowers the barrier and makes tunneling (emission) possible. The relationship between the emission current density and the applied electric field can be expressed as [12]

$$\ln(J/E^2) = \ln(A\beta^2/\phi) - B\phi^{3/2}/\beta E,$$

where A and B are two constants equal to $1.54 \times 10^{-6}\,(\mathrm{A \cdot eV \cdot V^{-2}})$ and $6.83 \times 10^9\,(\mathrm{eV^{-3/2} \cdot V \cdot m^{-1}})$, respectively, ϕ is the work function for electrons to get across the semiconductor-vacuum interface, which is about 5.3 eV for ZnO. β is a field enhancement factor. This relation is also known as Fowler-Nordheim equation. Based on the experimental data, we plot $\ln(J/E^2)$ *vs.* E^{-1}, as shown in the inset of fig. 5. A linear relationship between $\ln(J/E^2)$ and E^{-1} can be found, where the slope depends on ϕ and β. It can be seen that the multi-tip nano-prisms have the highest emission efficiency in all these cases.

The values of both turn-on field and threshold field for the nano-prisms with tines are lower than those of the nano-prisms without any tines atop. Moreover, E_{on} and E_{th} for the nano-prisms with multi-tips atop are lower than those with an individual tine. One possible explanation is that the multi-tined fish-spear–like nano-prisms possess multiple sites to generate electric current in comparision with the scenario of single-tine nano-prisms when the same voltage is applied across the electrodes. So with the same applied electric field, the field emission current from the fish-spear–like tips will be increased much faster and becomes much larger than that from the single-filament tips. Figure 5 indicates that longer and sharper nano-prisms require lower electric field in order to reach the same current density.

Figure 6 shows the typical CL spectra obtained at room temperature of the hierarchical ZnO nano-prisms by using spot mode scanning. All the spectra exhibit a UV emission at approximately 385 nm and a visible emission band centered at around 530 nm range from 450 to 650 nm. The 385 nm emission is conventionally attributed to the near band edge (NBE) ZnO emission, which is explained as the result of recombination of free excitons. In the visible emission band, the broadened peak can be decomposed into three emission peaks centered at about 490 nm, 540 nm, and 570 nm, respectively, as shown in fig. 6(b). It has been well established that the visible luminescence in ZnO mainly originates from the intrinsic defects states, such as oxygen vacancies [28], zinc

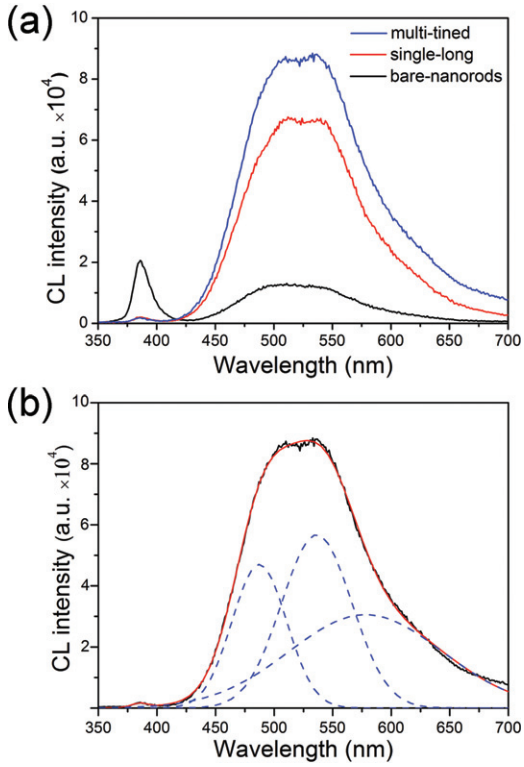

Fig. 6: (Colour on-line) Room temperature CL spectra of the ZnO nano-prisms with different tip morphologies. One may find that for the multi-tip nano-prisms the luminescence bump around 530 nm becomes dominant. (b) The CL spectrum of the nano-prisms with multi-tined filaments atop (black line), can be fitted by three Gaussian functions (blue dashed line). The combination of the Gaussian functions leads to a smooth curve (red solid line) that fits the experimental data reasonably well.

interstitials [29], zinc vacancies [30] and oxygen interstitials [31], especially from surface defect states [32,33]. First-principle calculations [34,35] show the most abundant native defects to be Zn and O vacancies depending on the Zn partial pressure. In Zn-rich conditions, oxygen vacancies and zinc interstitials have low formation energies. The UV emission of native nano-prisms is stronger than that of multi-tipped nano-prisms. On the contrary, the visible emission of the multi-tip nano-prisms is stronger than that of nano-prisms rods without any tines atop. These may be due to the better crystal quality of the nano-prism. When the oxygen supply is stopped, multi-tined nano-prisms are obtained. Meanwhile oxygen is deficient. Therefore, after cutting off the O_2 supply, more oxygen vacancies and zinc interstitials are generated in the tines atop nano-prisms and on nanorod surface, which contribute to the strong bump around 530 nm.

From the above results one may find that for field emission applications, it is beneficial to have multi-tip fish-spear–like ZnO nano-prisms in order to achieve the lower turn-on electric field and higher current density. For cathodoluminescence measurements, the multi-tip fish-spear–like ZnO nano-prisms may possess a large

amount of point defects, so the intrinsic lumminecence becomes relatively lower, yet the luminescence corresponding to defects becomes much stronger.

To summarize, we demonstrate in this letter that the tip morphology of the nano-prisms of ZnO can be controlled by changing the growth conditions. With the same amount of residue oxygen in the growth chamber, when the nitrogen flux is increased, the number of tines nucleated atop the nanorod gradually decreases. The relationship between the tine length and growth time is also studied. The field emission properties of nano-prisms with different tip morphologies are investigated. We find that the ZnO nano-prisms with multi-tines atop possess the lowest turn-on field and largest emission efficiency. Yet such multi-tipped nano-prisms have high defects density, which induces very strong cathodoluminescence around 530 nm. We suggest that our observations offer an interesting hint for optimizing the emission properties of nano-prisms.

* * *

The authors acknowledge the financial supports from the State Key Program for Basic Research from MOST of China (Grant No. 2010CB630705 and Grant No. 2012CB921502) and NSF of China (Grant Nos. 11204127, 11034005 and 61077023).

REFERENCES

[1] Xia Y., Yang P., Sun Y., Wu Y., Mayers B., Gates B., Yin Y., Kim F. and Yan H., *Adv. Mater.*, **15** (2003) 353.
[2] Barth S., Hernandez-Ramirez F., Holmes J. D. and Romano-Rodriguez A., *Prog. Mater. Sci.*, **55** (2010) 563.
[3] Wang Z. L., *Mater. Sci. Eng. Rep.*, **64** (2009) 33.
[4] Li Y., Qian F., Xiang J. and Lieber C. M., *Mater. Today*, **9**, issue No. 10 (2006) 18.
[5] Zhai T., Li L., Ma Y., Liao M., Wang X., Fang X., Yao J., Bando Y. and Golberg D., *Chem. Soc. Rev.*, **40** (2011) 2986.
[6] Fan S. S., Chapline M. G., Franklin N. R., Tombler T. W., Cassell A. M. and Dai H. J., *Science*, **283** (1999) 512.
[7] Chueh Y. L., Chou L. J., Cheng S. L., He J. H., Wu W. W. and Chen L. J., *Appl. Phys. Lett.*, **86** (2005) 133112.
[8] Au F. C. K., Wong K. W., Tang Y. H., Zhang Y. F., Bello I. and Lee S. T., *Appl. Phys. Lett.*, **75** (1999) 1700.
[9] Pan Z. W., Lai H. L., Au F. C. K., Duan X. F., Zhou W. Y., Shi W. S., Wang N., Lee C. S., Wong N. B., Lee S. T. and Xie S. S., *Adv. Mater.*, **12** (2000) 1186.
[10] Tondare V. N., Balasubramanian C., Shende S. V., Joag D. S., Godbole V. P., Bhoraskar S. V. and Bhadbhade M., *Appl. Phys. Lett.*, **80** (2002) 4813.
[11] Zhu Y. W., Zhang H. Z., Sun X. C., Feng S. Q., Xu J., Zhao Q., Xiang B., Wang R. M. and Yu D. P., *Appl. Phys. Lett.*, **83** (2003) 144.
[12] Wang W. Z., Zeng B. Q., Yang J., Poudel B., Huang J. Y., Naughton M. J. and Ren Z. F., *Adv. Mater.*, **18** (2006) 3275.
[13] Zeng H. B., Xu X. J., Bando Y., Gautam U. K., Zhai T. Y., Fang X. S., Liu B. D. and Golberg D., *Adv. Funct. Mater.*, **19** (2009) 3165.
[14] Wang Z. L., *Mater. Today*, **7**, issue No. 6 (2004) 26.
[15] Shu D.-J., Xiong X., Wang Z.-W., Zhang Z.-Y., Wang M. and Ming N.-B., *J. Phys. Chem. C*, **115** (2011) 31.
[16] Özgür Ü., Alivov Y. I., Liu C., Teke A., Reshchikov M. A., Dogan S., Avrutin V., Cho S. J. and Morkoc H., *J. Appl. Phys.*, **98** (2005) 041301.
[17] Wang Z. L. and Song J., *Science*, **312** (2006) 242.
[18] Zhao Q., Xu X. Y., Song X. F., Zhang X. Z., Yu D. P., Li C. P. and Guo L., *Appl. Phys. Lett.*, **88** (2006) 033102.
[19] Liu M., Ma G. B., Xiong X., Wang Z. W., Peng R. W., Zheng J. G., Shu D. J., Zhang Z. Y. and Wang M., *Phys. Rev. B*, **87** (2013) 085306.
[20] Fang X., Bando Y., Gautam U. K., Ye C. and Golberg D., *J. Mater. Chem.*, **18** (2008) 509.
[21] Liu C., Hu Z., Wu Q., Wang X. Z., Chen Y., Sang H., Zhu J. M., Deng S. Z. and Xu N. S., *J. Am. Chem. Soc.*, **127** (2005) 1318.
[22] Markov I. V., *Crystal Growth for Beginners*, 2nd edition (World Scientific, Singapore) 2003.
[23] Baxter J. B., Wu F. and Aydil E. S., *Appl. Phys. Lett.*, **83** (2003) 3797.
[24] Wang R. C., Liu C. P., Huang J. L., Chen S. J., Tseng Y. K. and Kung S. C., *Appl. Phys. Lett.*, **87** (2005) 013110.
[25] Shu D. J., Liu M. and Wang M., *Generic phase diagram of interfacial growth modes in homoepitaxy*, in preparation.
[26] Venables J. A., Spiller G. D. T. and Hanbucken M., *Rep. Prog. Phys.*, **47** (1984) 399.
[27] Fowler R. H. and Nordheim L., *Proc. R. Soc. London, Ser. A*, **119** (1928) 173.
[28] Klason P., Børseth T. M., Zhao Q. X., Svensson B. G., Kuznetzov A. Y., Bergman P. J. and Willander M., *Solid State Commun.*, **145** (2008) 321.
[29] Zhang S. B., Wei S.-H. and Zunger A., *Phys. Rev. B*, **63** (2001) 075205.
[30] Heo Y. W., Norton D. P. and Pearton S. J., *J. Appl. Phys.*, **98** (2005) 073502.
[31] Lin B., Fu Z. and Jia Y., *Appl. Phys. Lett.*, **79** (2001) 943.
[32] Wang Z. G., Zu X. T., Zhu S. and Wang L. M., *Physica E*, **35** (2006) 199.
[33] Wang R. C., Liu C. P., Huang J. L. and Chen S. J., *Appl. Phys. Lett.*, **86** (2005) 251104.
[34] Kohan A. F., Ceder G., Morgan D. and Van De Walle Chris G., *Phys. Rev. B*, **61** (2000) 15019.
[35] Erhart P., Klein A. and Albe K., *Phys. Rev. B*, **72** (2005) 085213.